Article

Not peer-reviewed version

Design and Implementation of Adaptive Deep Learning-Based DC-DC Converters for Photovoltaic Systems with Battery Storage in Electric Vehicles

Chitra Devi S * and A Ramkumar

Posted Date: 5 July 2024

doi: 10.20944/preprints202407.0545.v1

Keywords: Photovoltaic (PV) Systems; Battery Storage; Electric Vehicles (EVs); DC-DC Converters; Adaptive Deep Learning; Sliding Mode Control (SMC); Convolutional Neural Networks (CNN)

Article

Design and Implementation of Adaptive Deep Learning-Based DC-DC Converters for Photovoltaic Systems with Battery Storage in Electric Vehicles

S. Chitra Devi [1,*] and A. Ramkumar [2]

[1] Electrical and Electronics Engineering, Kalasalingam Academy of Research and Education, Krishnankoil, Srivilliputhur, Tamilnadu

[2] Electrical and Electronics Engineering, Kalasalingam Academy of Research and Education, Krishnankoil, Srivilliputhur, Tamilnadu; a.ramkumar@klu.ac.in

* Correspondence: schitradevi186@gmail.com

Abstract: Photovoltaic (PV) systems, which are renewable energy sources, are increasingly being utilized in distributed generation. To maintain a stable energy balance, energy storage systems such as batteries (BAT) play a vital role. Electric vehicles (EVs) offer a promising solution with rechargeable battery systems for operation. The BATs must maintain their state of charge within design boundaries, despite intermittent PV and load power fluctuations, and advanced power control and management techniques are essential for their effective operation. The article evaluates an intelligent controller that uses a Sliding Mode Control adaptive deep learning algorithm Convolutional Neural Networks (SMC-CNN) and a unique Strategy for managing supervisory power. (SPMS) for photovoltaic systems with battery energy storage for better regulation of DC bus voltage. SMC-CNN offers exceptional resilience and seamless functionality, minimizing fluctuations in DC bus voltage in the control strategy design requirements. The primary goals are maintaining a consistent power supply and ensuring continuous service by preventing system components from exceeding capacity. This study aims to enhance the control of DC bus voltage in the PV and battery system, with the primary significance focusing on the following aspects. The advanced SPMS has been created, incorporating control system constraints to enhance SOC balancing speed and reduce fluctuations in DC bus voltage. Power flow management involves optimizing energy flow between the PV system, battery system, and load while minimizing battery capacity requirements. The proposed SMC-CNN and SPMS are demonstrated through real-time simulation using Matlab/Simulink, as demonstrated in comprehensive case studies.

Keywords: photovoltaic (PV) systems; battery storage; electric vehicles (EVs); DC-DC converters; adaptive deep learning; sliding mode control (SMC); convolutional neural networks (CNN)

1. Introduction

The growing demand for environmentally friendly and accessible power solutions is driven by concerns over greenhouse gas emissions and pollution from thermal power plants and nuclear facilities. The development of a high-performing, reliable, and affordable battery charger for electric vehicles (EVs) is a top priority, requiring an AC-DC converter to meet system requirements. The pursuit of eco-friendly energy solutions, particularly in EVs, is largely driven by advanced technologies like AC-DC converters. he study presents a DC-DC converter with a customized PI controller, designed to achieve target output voltage and high current density, reducing overshoot in a lithium-ion battery setup.

The primary objective is to reduce the charging time significantly [1]. The research presents a dual-directional DC-DC converter with a high amplification factor, ideal for integrating energy storage units with electric cars, using minimal components and duty cycle functions. [2].This study proposes a novel configuration for DC-DC converters that are not isolated, utilizing voltage boost technique principles for high gain and low voltage applications [3]. The study explores an experimental hybrid micro grid system, combining renewable energy sources like Wind Generator, Solar Array, Fuel Cell, and Energy Storage System with a battery for remote areas [4]. The paper

 doi:10.20944/preprints202407.0545.v1

introduces a novel bidirectional switched Z-source DC-DC converter that effectively boosts voltage using a switched-capacitor methodology and inductors.

It also offers There is a broad spectrum of duty cycles available in both boost and buck modes, resulting in a substantial voltage conversion ratio [5].The paper proposes various topologies of DC/DC converters, enhancing the efficiency and range of electric sports cars by adjusting the inverter's input voltage to various torque/speed conditions and utilizing Instead of utilizing SVPWM, synchronous modulation methods are employed within the WLTC [6].This study explores resonant converter configurations, operational modes, modeling, control strategies, and unique design considerations, focusing on current topologies and control methods to create novel converter configurations and approaches[7]. The research introduces a non-isolated multi-port power converter for electric vehicles, enabling the integration of various energy sources, improving load power allocation, and enhancing energy efficiency [8]. The article examines the operation of a resonant tank power converter in electric vehicle applications, highlighting zero-voltage switching as a crucial technique for improving efficiency and reducing switching losses [9]. This study investigates three-phase bidirectional/DC converters and DC/DC isolated full bridge converters, focusing on unity power factor control and dual active power control for EV battery charging and discharging.

[10]. In this study of ACL type isolated dc-dc converters for safety and reliability in energy conversion applications is extensive, but their dynamic equivalence remains unsystematically understood.

[11].Renewable energy sources, primarily solar and wind power, are being utilized for power generation and installed in electrical systems [12]. Dynamic power management structures are widely used to integrate renewable energy sources and energy storage systems into DC buses.

. [13–14]. Research papers have extensively explored the energy management system (EMS) in various applications of hybrid PV-BAT systems, including electric vehicles, charging stations, electricity, and smart microgrids [15]. Research papers explore energy management systems (EMS) in hybrid PV-BAT systems, comparing power management strategies and architectures for electric vehicles, charging stations, electricity, and smart micro grids.

[16–17**].** The study proposes various power management techniques for hybrid PV-BAT systems in off-grid residential households.

. [18-19]. Researchers propose the utilization of multiple sophisticated control techniques in order to meet various objectives within the realm of Energy Management Systems (EMSs). The development of EMSs involves the incorporation of a wide range of fields, such as linear and nonlinear algorithms. [20-22]. Recent research has proposed several control strategies for voltage, frequency regulation, and power management, including PI/PID linear controllers, fuzzy logic controllers (FLC), and artificial neural network controllers. [23]. Comparative studies on online EMS will evaluate passive controllers and finite-state machine controllers, focusing on optimizing fuzzy control algorithm's superior functionality in hybrid power systems [24].

The study proposes a fuzzy-tuned dynamic PI controller to regulate the high power content of the flywheel and supercapacitor using integrated state variables [25].

This research paper investigates energy management in a DC microgrid, focusing on controlling limits and managing energy saturation. It examines distributing power loads based on ratings, regenerative braking, and regulating DC bus voltage to ensure power load fulfillment [26].

The study introduces a novel PV-BAT system using adaptive CNN-based control and EMS, suitable for various industrial sectors; especially DC micro grids. The new EMS framework enhances supervisory control for power management, enhancing efficiency, security, and system performance by integrating control system constraints to improve energy balance.

A controller-based CNN with adaptive parameters improves DC bus voltage regulation, addressing system nonlinearities and reducing instability. An anti-windup compensator maintains linear range and optimal battery performance.A basic power flow management system enhances efficiency by minimizing component constraints and utilizing a straightforward structure to manage operations between PV units, BAT units, and loads. The study suggests using MATLAB/Simulink and microcontroller for simulation and experimentation is to ensure reliable energy delivery in

 doi:10.20944/preprints202407.0545.v1

unforeseen situations by improving state of charge equilibrium and minimizing direct current bus voltage variations.

2. System Description

2.1. System Architecture

A parallel structured hybrid system utilizes photovoltaic panels as its main power source, with storage systems serving as an additional source of energy.As depicted in Figure 1, the control devices of DC-DC static converters regulate power to meet load demands.

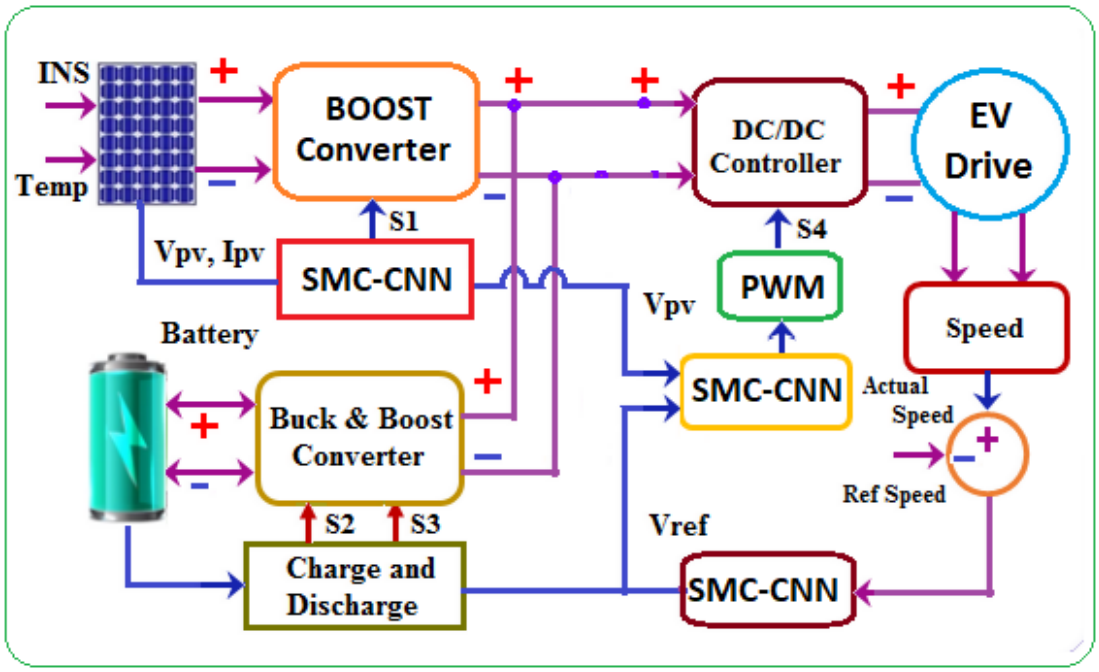

Figure 1. Typical hybrid architecture of the PV/BAT EV systems.

The four primary components of a hybrid system are photovoltaic generation units, battery-based energy storage systems, and electric vehicle loads. The primary source and ancillary device must complement each other, and converter selection and dimensions are determined by PV and BAT unit behavior, load profile, and application.

$$\eta_{Load} P_{Load}(t) = \eta_{PV} P_{PV}(t) + \eta_{bat} P_{bat}(t) \quad (1)$$

where;

η_{PV} -Efficiency of the PV Panel

η_{bat} -Efficiency of the Battery

η_{Load} - Efficiency of the Load

The examination concentrates on the DC converters associated with the PV array, batteries, and loads. The investigation presupposes a mean effectiveness of the power converters.

2.2. Modeling of Systems

2.2.1. PV Model

This study uses mono-crystalline silicon photovoltaic modules with a single-diode model and a series resistor to account for intra-cell losses.

Preprints.org (www.preprints.org) | NOT PEER-REVIEWED | Posted: 5 July 2024 doi:10.20944/preprints202407.0545.v1

$$I_{PV} = I_{ph} - I_d\left[\exp\left(\frac{q\left(V_{pv} + R_s I_{PV}\right)}{nkT}\right) - 1\right] - \frac{V_{PV} + R_s I_{PV}}{R_{sh}} \quad (2)$$

$$I_{PVarry} = N_p I_{pv} \quad (3)$$

$$R_{arry} = \frac{N_s}{N_P}(R_s + R_{sh}) \quad (4)$$

Mono-crystalline silicon PV modules use a single-diode model with a series resistor, incorporating Boltzmann's constant and surface temperature, with "k" representing losses. A PV array model can be represented by whereNs symbolizes a number of series-connected modulesand Np represent a number of parallel-connected modules.

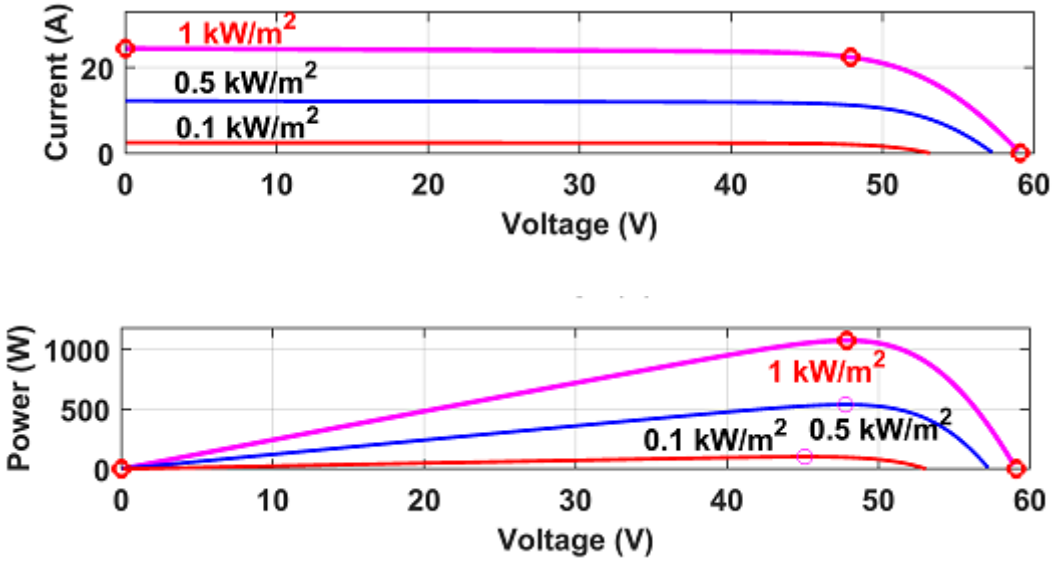

Figure 2. PV Characteritics (a) IV (b)PV.

2.2.2. Model of Battery.

This study utilized a standardized model of a lead-acid battery (BAT) to evaluate two key factors: terminal voltage (BAT) and state of charge (SOC). The model includes the open-circuit voltage (E0), battery capacity (Ah), internal resistance, polarization voltage (K), exponential voltage (A), and exponential capacity (B).

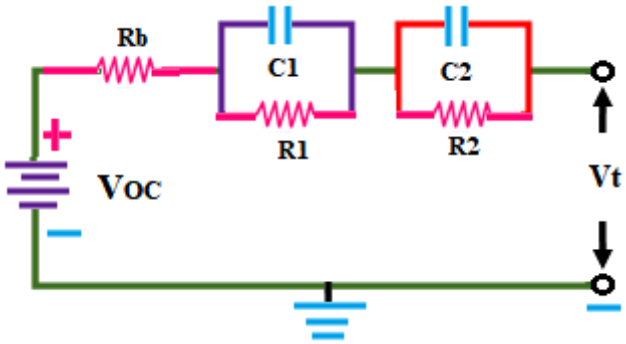

Figure 3. Equivalent of battery.

 doi:10.20944/preprints202407.0545.v1

2.2.3. PV Boost Converters

Depicted in Figure 1.5, A boost converter is a DC-DC power converter that increases input voltage by harnessing energy in an inductor and delivering it to the output, thereby achieving higher output voltages.

This paper employs a boost converter, as shown in Figure 4, to achieve its objectives. The key equation provided is essential for calculating the duty cycle needed to operate the transistor's gate at the maximum power point

$$V_o = \frac{V_i}{1-D} \tag{5}$$

The boost converter in PV applications must adjust the duty cycle (D) to maintain the maximum power point of the PV array under fluctuating environmental conditions:

1. This research paper utilizes a boost converter, depicted in Figure 4, to achieve its objectives. The equation provided below plays a crucial role in determining the duty cycle required to operate the gate of the transistor at the maximum power point.

$$L \geq \frac{(1-D)^2 DR}{2 f_{SW}} \tag{6}$$

b. The value of the input capacitor C_{in} can be calculated by:

$$C_{in} = \frac{I_o D^2}{0.02(1-D)V_{in} f_{SW}} \tag{7}$$

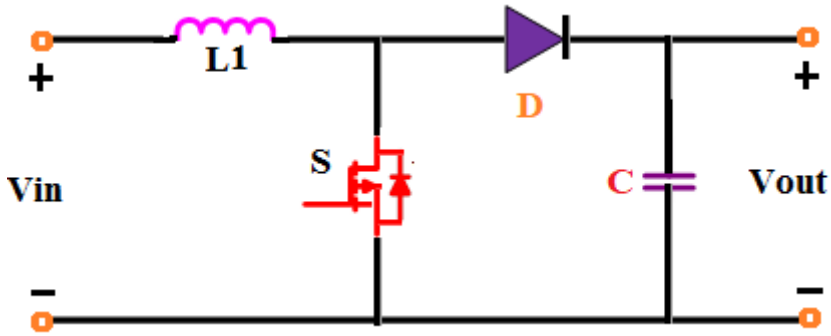

Figure 4. Boost Converter.

To maintain input voltage stability in a switching power supply, the minimum input capacitor value is determined based on peak current requirements. The output capacitor should handle load current and exceed converter output voltage, with ripple voltage below 3%:

$$C_{out} = \frac{DV_o}{V_r R f_{SW}} \tag{8}$$

The boost converter parameters necessary to achieve a maximum power output of 100 KW from the PV generator are detailed in Table 2, where D represents the duty cycle, R signifies the resistance of the load, f sw denotes the switching frequency, Io stands for the output current, Vin represents the input voltage, Vo indicates the output voltage, and Vr represents the capacitor ripple voltage.

A boost converter consists of an inductor, diode, capacitor, and switch. The switch operates by connecting input voltage to the inductor during charging and disconnecting it during discharging, transferring stored energy to the output, resulting in higher output voltage.

 doi:10.20944/preprints202407.0545.v1

2.2.4. Battery Buck-Boost Converter

The buck-boost converter functions as a DC to DC converter, where the output voltage can either be lower or higher than the input voltage. The magnitude of the output voltage is determined by the duty cycle. Step-up and step-down transformers are converters that are named after the analogous transformers. The input voltages undergo step-up or step-down conversion, utilizing minimal conversion energy to achieve input power equivalent to output power, as illustrated in the equation.

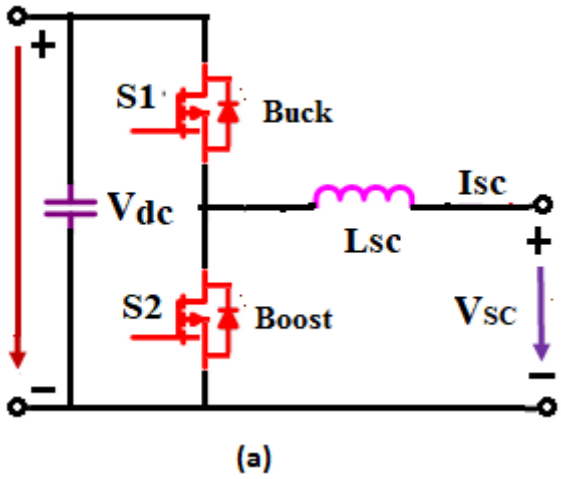

Figure 5. Bi-directional Converter.

2.3. System Operation

The PV-BAT system operates in either charge or discharge mode, depending on the power availability. Long-term power imbalances can cause deep discharging or overcharging. To maximize BAT lifespan and PV power generation, the system can be categorized into normal mode, which involves regular charging and discharge, and transient mode, which involves complete charge/discharge.

2.3.1. Stable Operation

Charge modeCharge mode: The photovoltaic system's power output exceeds the load's demand, resulting in a lower State of Charge than the maximum capacity, excess power is stored in the battery using a bidirectional converter in charge mode, ensuring efficient renewable energy utilization.

$$P_{BAT} = P_{pv} - P_{LOAD} \quad (9)$$

2. **Dischargemode:** The PV system's load consumption exceeds its power generation, requiring the battery (BAT) to supply additional energy. The bidirectional converter operates in discharge mode to offset the DC bus power deficit.

$$P_{LOAD} = P_{PV} + P_{BAT} \quad (10)$$

2.3.2. Transient Mode

The PV power generation has not reached its maximum threshold, and the battery is nearing its maximum charge. The BAT controller prevents overcharging by transitioning the system to DC bus voltage regulation.

$$p_{PV} = P_{LOAD} \quad (11)$$

Preprints.org (www.preprints.org) | NOT PEER-REVIEWED | Posted: 5 July 2024 doi:10.20944/preprints202407.0545.v1

The photovoltaic power output is insufficient for load demand, requiring a battery controller to prevent deep discharge and disconnect non-essential loads for power equilibrium and DC bus stability.

$$PLoad \approx PPV \quad (12)$$

Recharging/discharging of the BAT stops when they are fully charged/discharged.

3. SPMS

By using simulation block sets for logical switching (ON and OFF), the suggested SPMS controller algorithm is implemented. The controller monitors the Ppv, Battery power and compares it to the power at load(P_{load}). If the consumption is lower than the Ppv, extra power is delivered to a storage device. The load demands more power from the Battery stack than the PV system can provide. Figure 7 show the switching mechanism for the three separate SMC-CNN system controllers.

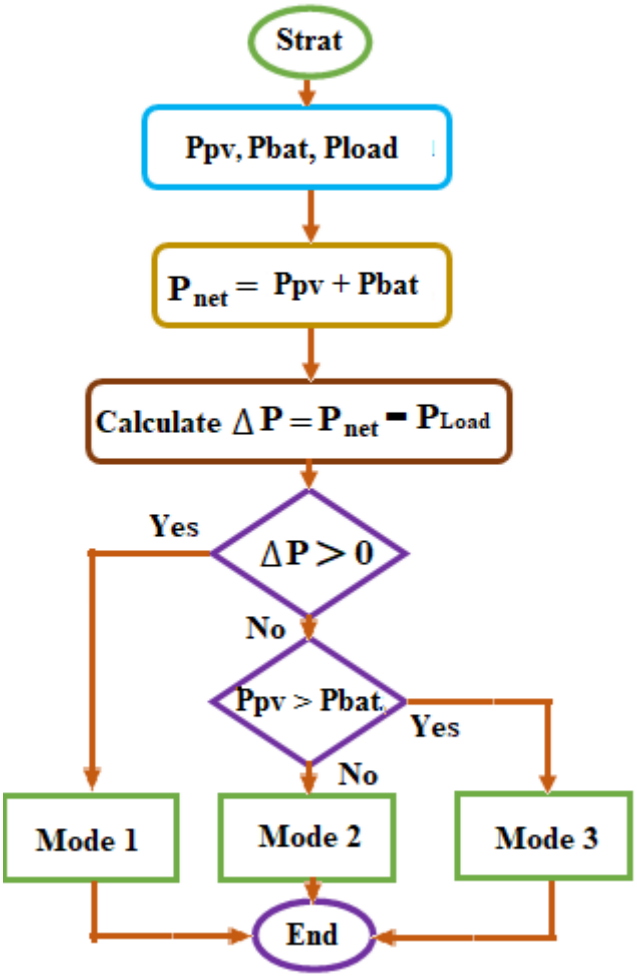

Figure 6. EMS system.

Mode 1: In this scenario, the photovoltaic power generated exceeds the amount required to meet the load demand($P_{pv} > P_{load}$).

In this particular case, the power generated by the photovoltaic system(P_{PV}) falls short ($0 < P_{PV} < P_{load}$), thus requiring the utilization of fuel cells to fulfill the power requirements. This compensating mode ensures that the power demand is met by combining the power from the photovoltaic system and the battery.

$$\left(P_{load} = P_{pv} + P_{bat}\right) \quad (13)$$

Preprints.org (www.preprints.org) | NOT PEER-REVIEWED | Posted: 5 July 2024 doi:10.20944/preprints202407.0545.v1

Mode 2: This mode is active when the PV generator supplies the energy($Ppv > Pbat$)so battery added to Ppvtosupply the load ($P_{Load} = P_{bat}$).

Mode 3: In this case ($Ppv < P_{bat}$)hence the battery added to P_{pv} to supply the load

$$\left(P_{Load} = P_{pv} + P_{bat}\right) \quad (14)$$

3.1. SMC Control

The sliding mode control technique is a nonlinear control strategy used to create robust controllers for complex, high-order, nonlinear dynamic systems in uncertain environments. One of the key elements of sliding mode control is the establishment of a sliding surface within the state space of the system. The procedure involves selecting a control law to guide the system towards a specific surface, and incorporating appropriate switching logic to maintain proximity.

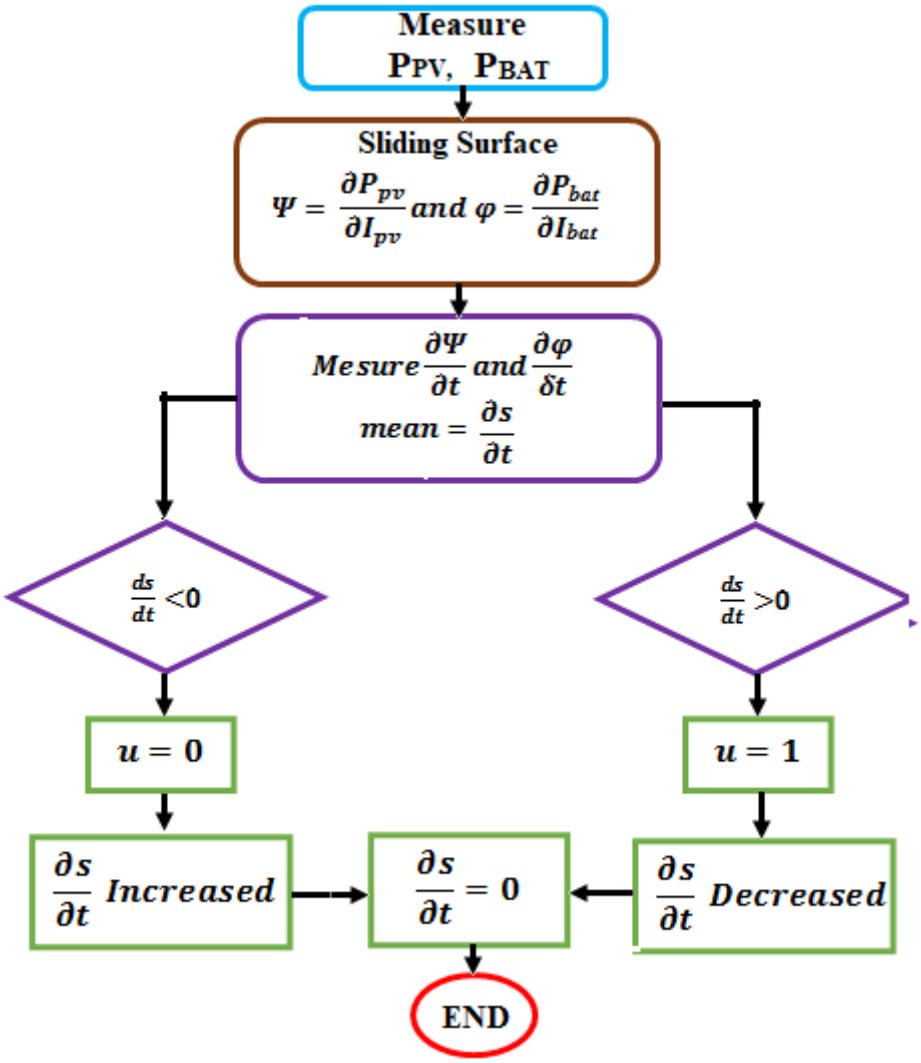

Figure 7. SMC controller.

The utilization of the Sliding Mode Control (SMC) technique in conjunction with the Photovoltaic (PV) system is demonstrated in this study. The dynamic response of the DC/DC boost converter is influenced by the signal (u), which allows the SMC method to exert control over the switch of the boost converter transistor. The model provided accurately captures the behavior of the system.

$$\psi = \frac{\partial P_{PV}}{\partial t}, \phi = \frac{\partial P_{bac}}{\partial t} = \frac{\partial s}{\partial t}\phi \quad (15)$$

Where P_{PV}, $Pbat$, Power Sources of the system.

 doi:10.20944/preprints202407.0545.v1

The PV power (P_{pv}) and BAT power (P_{bat}) are found as

$$P_{pv} = V_{pv} I_{pv}, P_{bat} = V_{bat} I_{bat} \quad (16)$$

Based on equation (2), the Sliding surface of the system is presented in equations (3) and (4).

$$\frac{\partial P_{source}}{\partial I_{source}} = V_{Source} + I_{Source} \frac{\partial V_{Source}}{\partial I_{Source}} \quad (17)$$

$$s = V_{source} + I_{source} \frac{\partial V_{source}}{\partial I_{source}} \quad (18)$$

Where s, σ, φ, ψ sliding surface of PV, wind, SC and grid respectively

The control parameter of the SMC is obtained from equations (1) - (4).

The equation demonstrates that SMC can be represented by a unique duty cycle (d). (5),

$$d = v + ksign(s) \quad (19)$$

The visequivalent control value, calculated using equation (6) as k is the gain constant, therefore,

$$v = 1 - \frac{Vsource}{V_{dc}}, \quad (20)$$

The duty cycle range fluctuates from 0 to 1, thereby imposing certain limitations.

SMC logic are presented in equation (7),

$$d = \begin{cases} 1\, v_{Source} + ksign(s) > 0 \\ 0 v_{Source} + ksign(s) < 0 \end{cases}, \quad (21)$$

The SMC controller finds the optimal operating point of the surface and compares with common dc bus voltage and produces the modulation index (MI). After that, the PWM signal employs a comparator to generate a control pulse with operating at a frequency of 3000 kHz and a

3.2. SMC-CNN Control

Convolutional Neural Network (CNN) represents a sophisticated form of Artificial Neural Network (ANN) specifically designed to handle time-series dataarchitecture shown in Figure 9. The CNN architecture comprises three essential layers: The convolution layer, pooling layer, and fully-connected layer each serve distinct roles in a convolution neural network. Specifically, the convolution layer is designed to capture local features within the input data, while the pooling layer works to reduce the dimensionality of the input data.

Preprints.org (www.preprints.org) | NOT PEER-REVIEWED | Posted: 5 July 2024 doi:10.20944/preprints202407.0545.v1

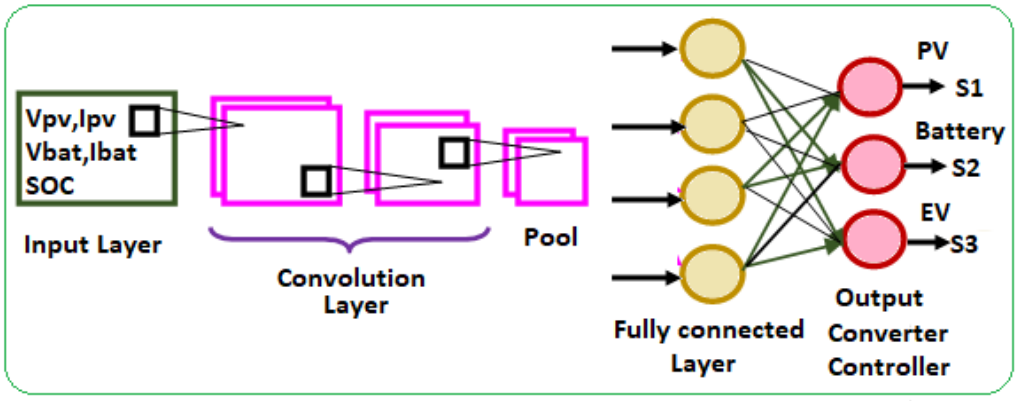

Figure 8. Architecture ofCNN.

The prediction of outputs is accomplished by utilizing the extracted features in the fully-connected layer. The convolution, which refers to the processing of the extracted local spatial variables and their connections with the input variables, can be represented by the following equation:

$$C_i = f\left(x \otimes \omega_i + b_j\right) \tag{22}$$

The inputs for the CNN are denoted by x.;
The symbol Ci represents the local feature corresponding to the ith output of the convolution layer;
⊗- representsconvolution operation;
The current study opts for the nonlinear activation function ReLu to serve as the activation function f (·) within this particular model, with ReLu being mathematically represented as Eq. (23);

$$f(z) = ReLu\begin{cases}0, & if\ -z \le 0\\ z, & if\ \ z > 0\end{cases} \tag{23}$$

The bias matrix is denoted by b, where b_j and ω_i denote the bias of the initial weight matrix and convolution kernel of the convolution layer, respectively; i represents the total number of convolution kernels.

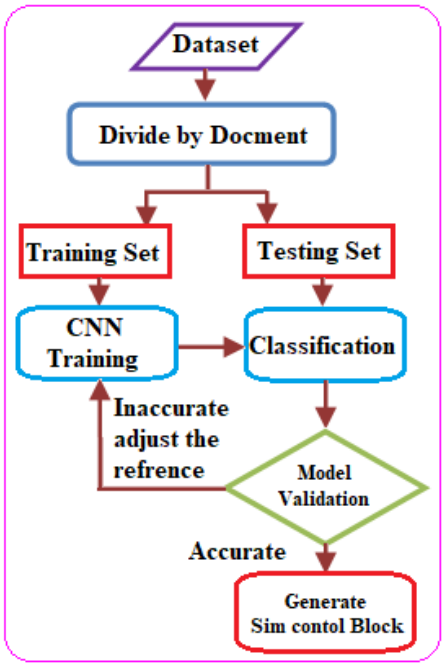

Figure 9. CNN Functional flow chart.

Preprints.org (www.preprints.org) | NOT PEER-REVIEWED | Posted: 5 July 2024 doi:10.20944/preprints202407.0545.v1

The database utilized in this study comprises 5000 patterns of PV voltage, PV current, battery voltage, current, SOC, EV drive parameters such as speed and reference voltage variables. This database has been split into two sub-databases, with 70% of the samples allocated for training the CNN, while the remaining 30% are utilized for testing and validating the network. Figure 10 depicts the operational flow diagram of the CNN.The selected training sets aim to encompass the entire standard input range to achieve optimal performance, with a consistent temperature of 25°C and solar irradiation levels varying between 50 W/m² and 1050 W/m².

4. Simulation Result

The power management systems based on Matlab/Simulink and Proposed SMC-CNN, illustrated in Figure 10, have been intricately crafted. PV and BAT systems are integrated with their respective DC-DC power converters within these systems. Furthermore, each unit integrates a DC bus and an electric vehicle (EV) DC Drive, both equipped with advanced control systems. SMC-CNN's power management system monitors PV and BAT power sources, fulfills load demands, and ensures efficiency. Voltage stabilization capacitor smooths voltage fluctuations, reducing bus voltage ripple. The modulation index must be adjusted continuously to maintain stable output voltage in a PV array, particularly during decreased sunlight and input voltage drop.

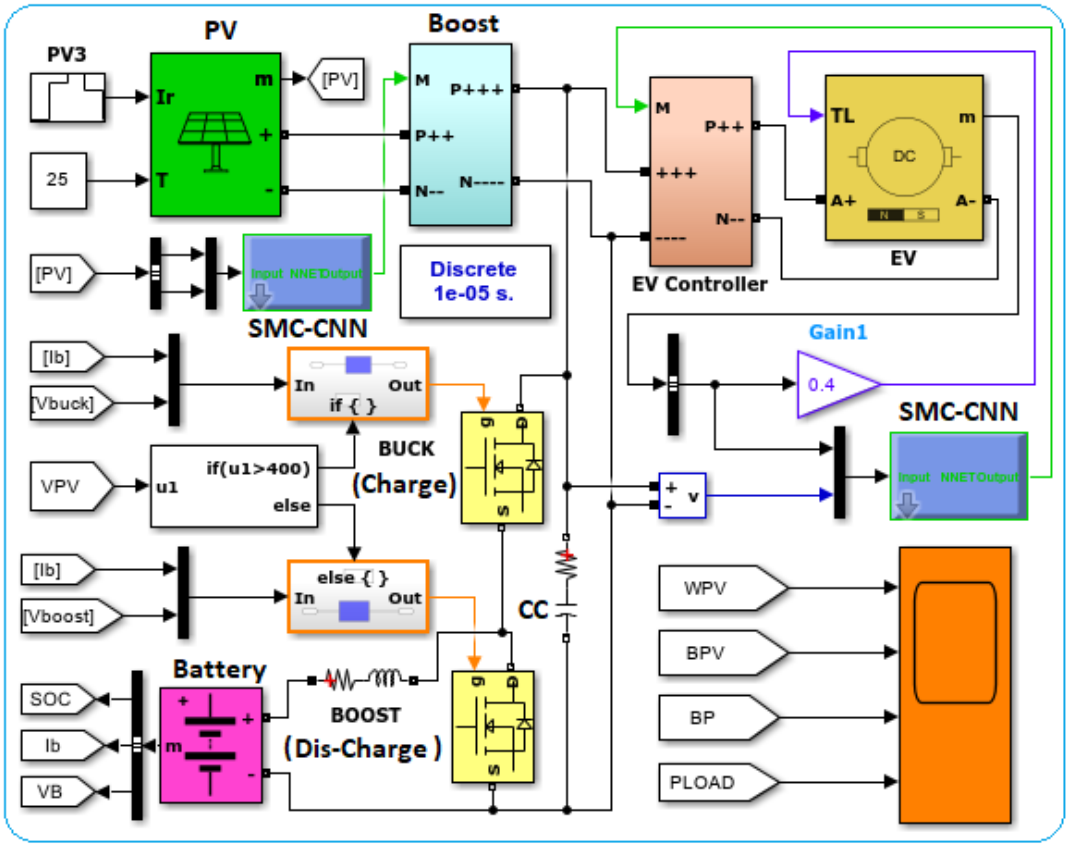

Figure 10. Simulation Model of PV/BAT EV systems.

Converter Output Voltage Stability a well-designed PMS controller maintains converter output voltage stability by real-time adjusting modulation index and compensating for non-idealities in converter components. The converter's robust design, low-voltage ripple, and efficient control algorithms demonstrate its ability to handle transients effectively. The DC bus link capacitor is a crucial component in multi-converter systems, acting as a buffer to prevent short-term disturbances, ensuring system stability and performance.In consideration of a specific situation, the solar irradiance fluctuates within a predetermined range, with subsequent adjustments in charge and discharge configurations gradually decreasing to a specified minimum level, as illustrated in Table 5. In order to replicate a real- time scenario, the progressive alteration in irradiation is visually depicted in Figure 11.

Preprints.org (www.preprints.org) | NOT PEER-REVIEWED | Posted: 5 July 2024 doi:10.20944/preprints202407.0545.v1

Table 5. Simulation Configuration.

Operational time		Insolation(w/m²)	BATe(V_{dc})
Pattern	Duration		
SP1	0.0s-0.6s	0-200-380	Discharge
SP2	0.6s-1.6s	380-720-390	Charge
SP3	1.6s-2.0s	390-220-0	Discharge

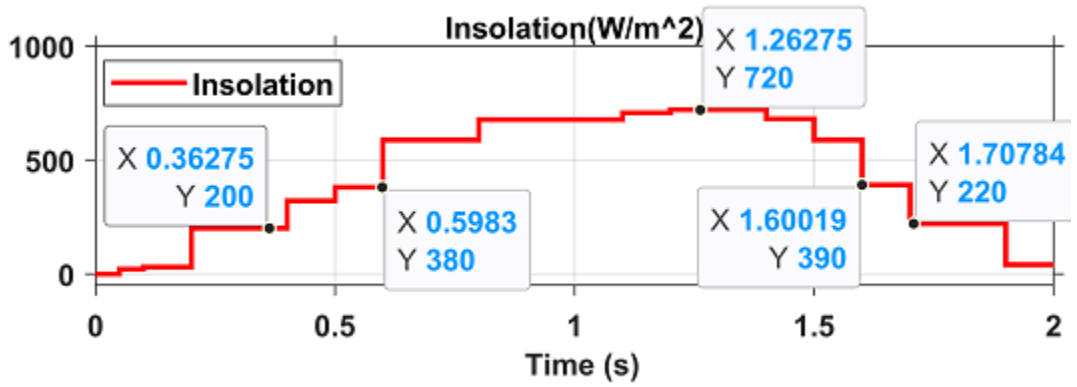

Figure 11. PV Insulations.

The various configurations showcased a range of patterns and scenarios present in the system, providing a comprehensive evaluation of how well the proposed scheme performs in different situations. Simulations were conducted to evaluate the effectiveness of these algorithms, covering a time frame from 0 seconds to 2.0 seconds, with a particular emphasis on electric vehicle (EV) propulsion and its critical load applications.

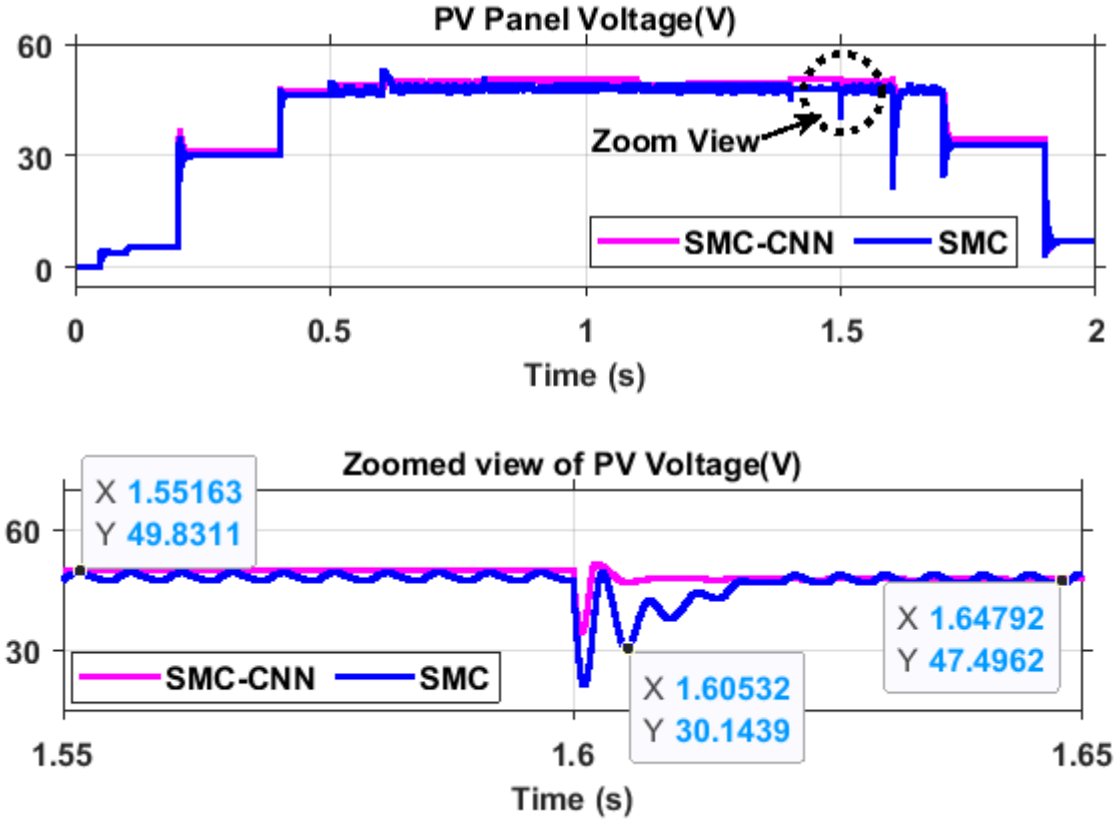

Figure 12. (a) PV Panel Voltage,(b) Zoom View.

Preprints.org (www.preprints.org) | NOT PEER-REVIEWED | Posted: 5 July 2024 doi:10.20944/preprints202407.0545.v1

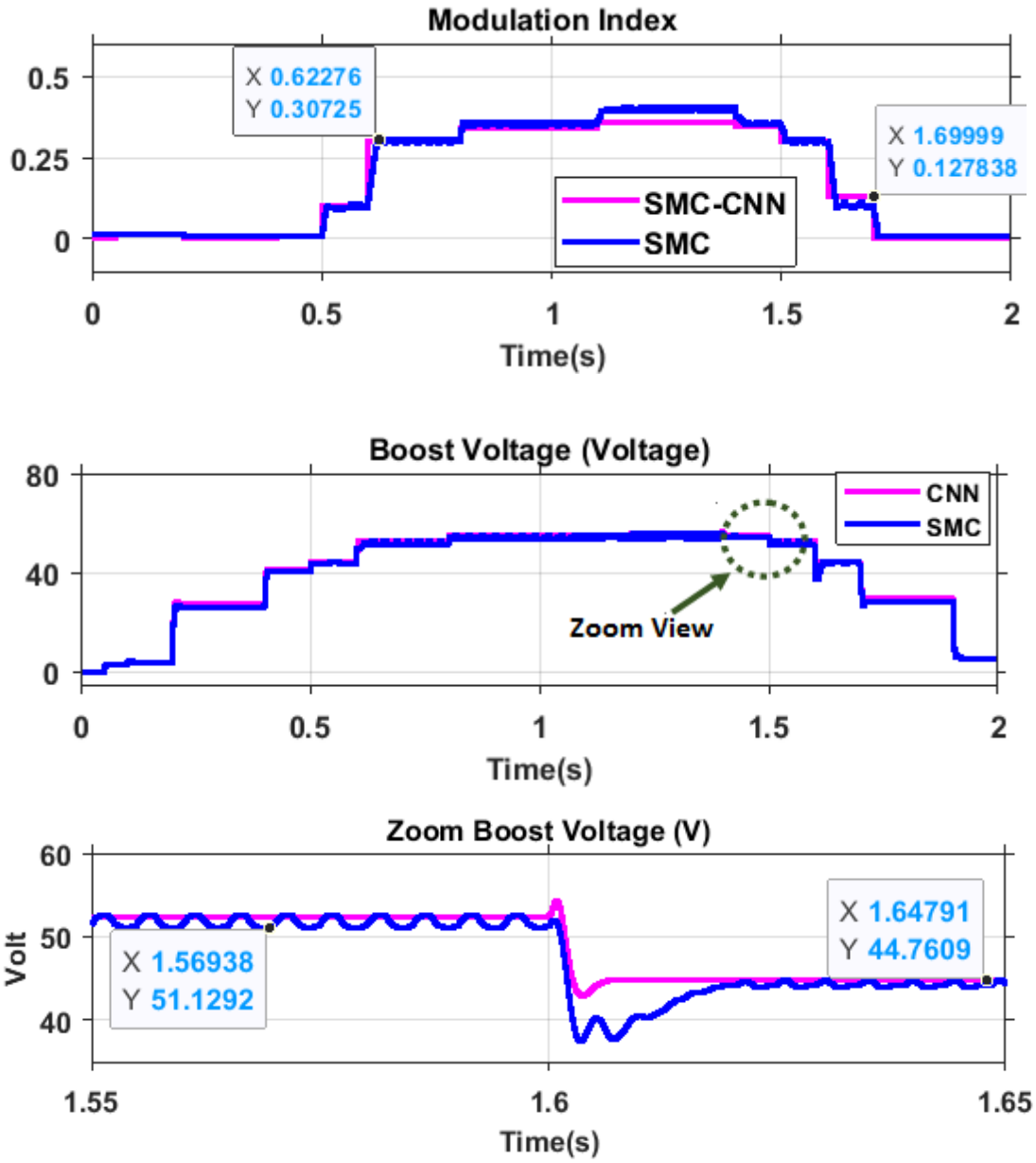

Figure 13. (a) PV Panel Voltage ,(b) Modulation Index (c) Boost voltage (d) Zoom view of boost voltage.

The study examines the effectiveness of different photovoltaic inputs under different atmospheric conditions, as well as the impact of environmental challenges and the availability of backup battery resources. This is achieved by implementing a suggested power management algorithm controller. Throughout the research, the simulation analysis focuses primarily on steady-state performance metrics. These metrics include load current, voltage ripple amplitudes, overshoot, and settling time duration. The analysis takes into account the dynamically changing insolation and the charge and discharge mode of operation.

Figure 12 (a)-(b) illustrates the corresponding simulated source parameter of PV panel voltage .Figure 13(a)-(b) presented modulation Index and converter output voltage and its zoomed version.

Figures 13 (a-b) provide a comprehensive depiction of the crucial elements involved in the operation of a PV boost DC/DC converter. The modulation control strategy, the detailed analysis of the output voltage performance, and the stabilizing effect of the DC bus capacitor are all encompassed within the system. These illustrations emphasize the significance of meticulous control and resilient design in attaining both efficient and stable power conversion in PV systems.

PV power 14 (a)-(b) The shared DC bus inverter capacitor is an essential element in systems where multiple converters or power sources contribute to a common DC bus. Its primary function is

Preprints.org (www.preprints.org) | NOT PEER-REVIEWED | Posted: 5 July 2024 doi:10.20944/preprints202407.0545.v1

to ensure voltage stability on the DC bus by absorbing transients and delivering a consistent voltage level to downstream

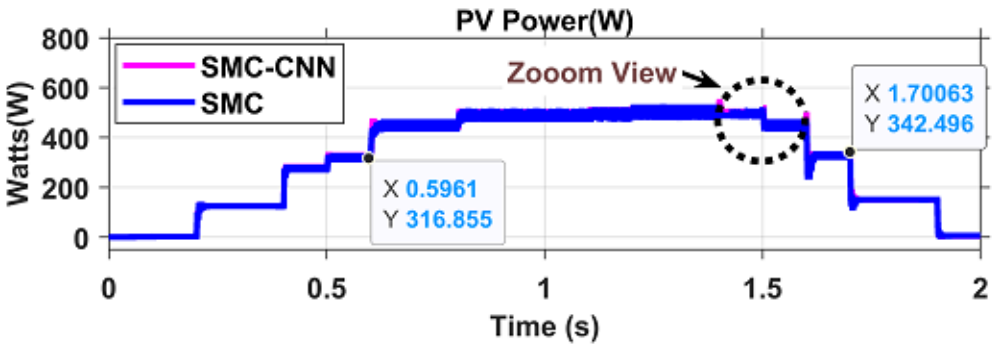

devices.

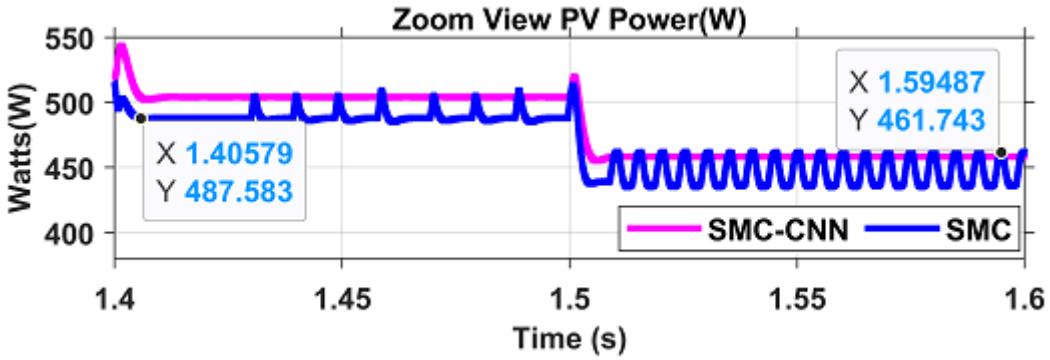

Figure 14. (a) PV Load Power (b) Zoom View.

Figure 15(b-c) illustrates the anticipated power of the battery (W), showcasing the power response of the rear source battery. By examining the fluctuations in power, which is the outcome of multiplying voltage and current, the energy transfer to or from the battery can be determined. The zoomed-in view of Figure 15(b) provides a closer analysis of these variations.

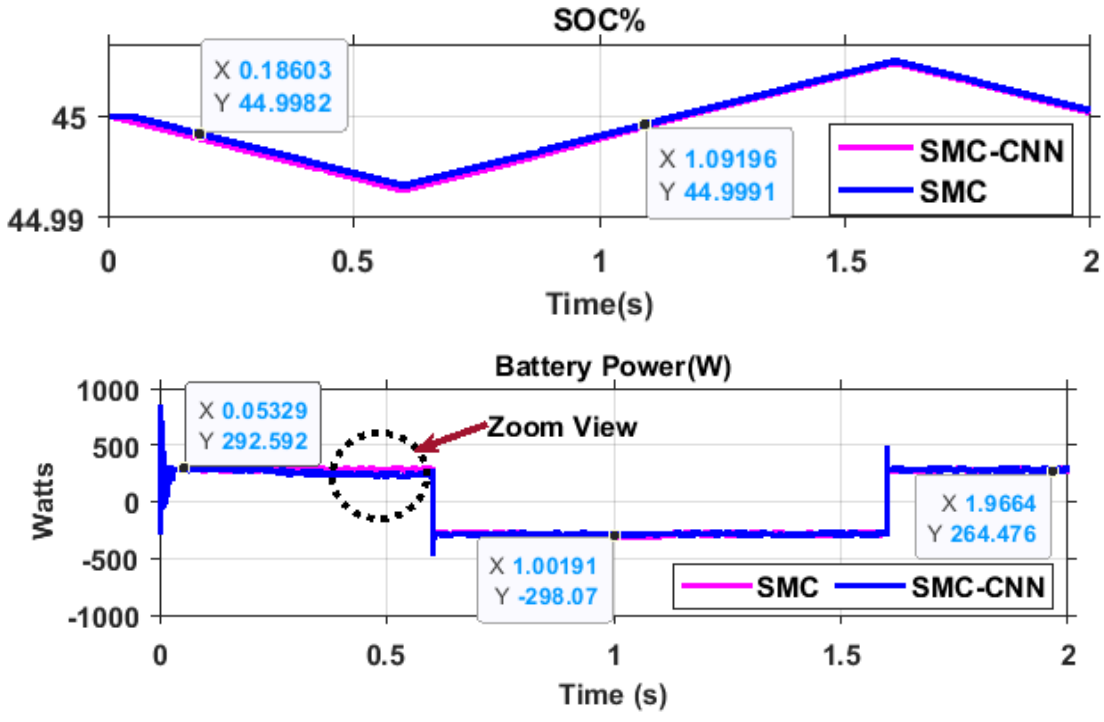

Preprints.org (www.preprints.org) | NOT PEER-REVIEWED | Posted: 5 July 2024 doi:10.20944/preprints202407.0545.v1

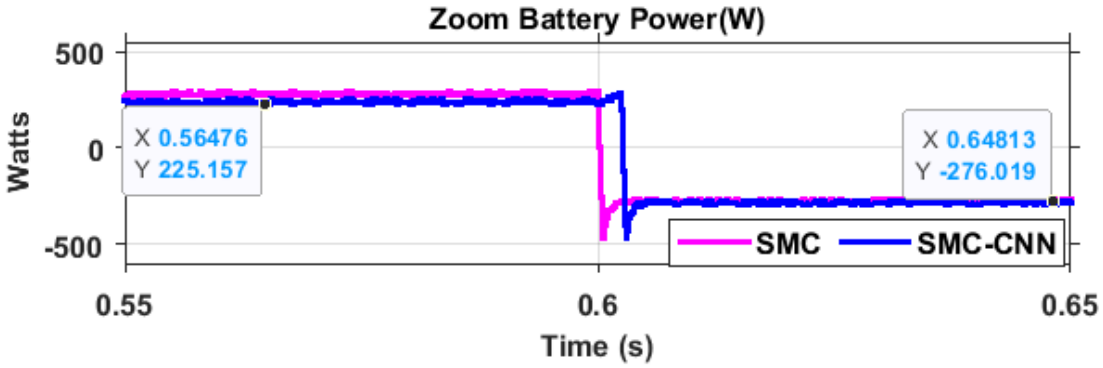

Figure 15. (a)SOC Battery (b) Charge and Discharge power(c) Zoom view of power.

Figure 15(b-c) illustrates the anticipated power of the battery (W), showcasing the power response of the rear source battery. By examining the fluctuations in power, which is the outcome of multiplying voltage and current, the energy transfer to or from the battery can be determined. The zoomed-in view of Figure 15(b) provides a closer analysis of these variations.

The examination goes deeper into the drive load voltage, load current torque, and drive speed values of the three main configurations of SMC and SMC-CNN, as shown in Figures 8 and 9. It is important to highlight that the torque and speed values are recorded at 230.9, 199.20, 231.45, and 199.50 for SMC, demonstrating significant differences when compared to SMC-**CNN controller.**

The conventional SMC controller's performance is evaluated by monitoring the transient values of voltage, current, and power until reaching a steady-state at 0.0965s. The observed values at steady-state are 619.80W for the auxiliary DC drive and 659.92W for the main DC drive. The duration of the period for battery charge mode operation is also determined. During the SP2 (0.6s to 1.6s) pattern, the PV insolation pattern shifted from 380, 587, 677, 706, 720, 680, and 587 to a different sequence. Throughout this period, when the PV power exceeded the load power, the surplus energy was stored in the battery. The PV power was utilized to manage both the EV Drive battery.

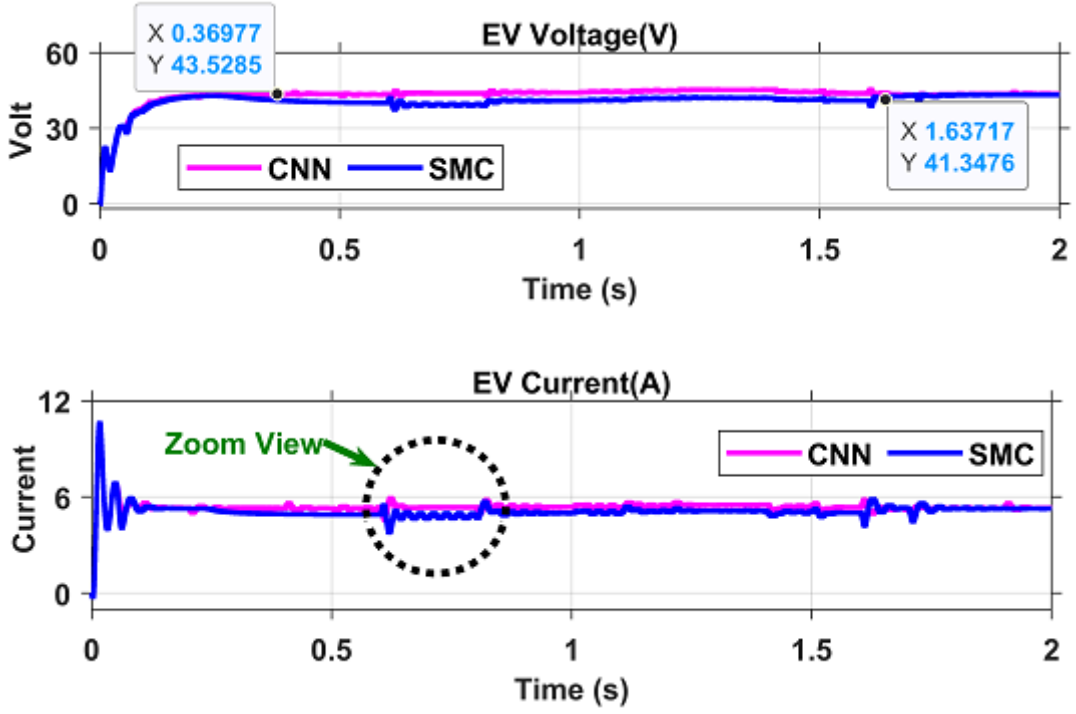

Preprints.org (www.preprints.org) | NOT PEER-REVIEWED | Posted: 5 July 2024 doi:10.20944/preprints202407.0545.v1

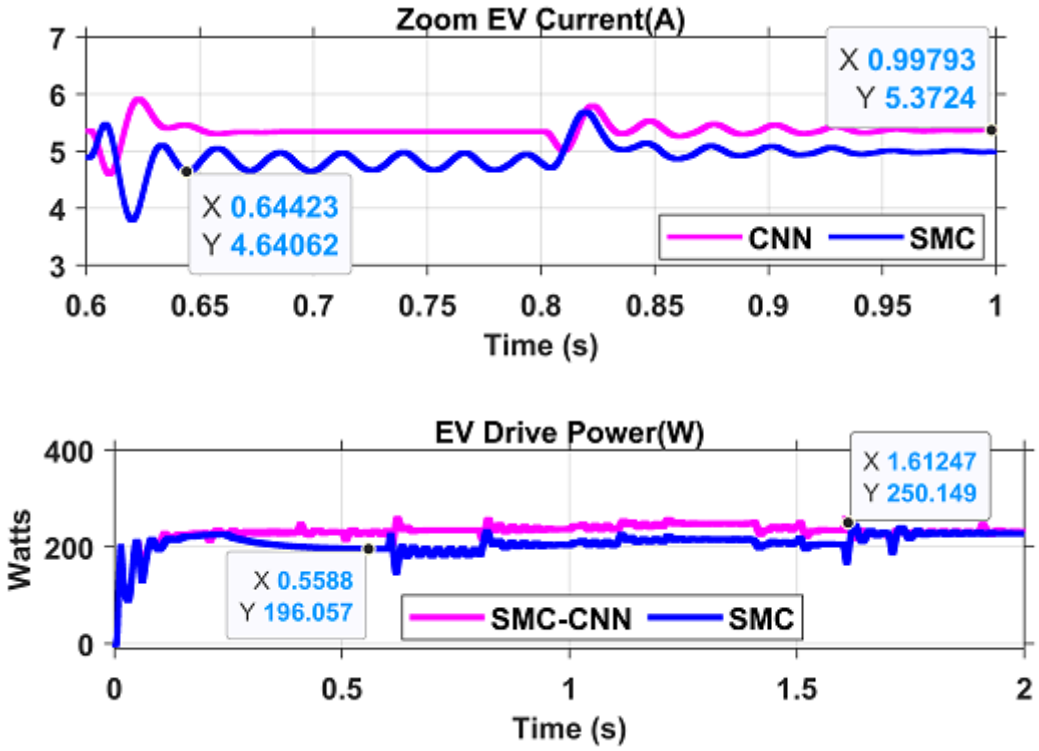

Figure 16. EV Parameter (a) Voltage (b) Current (c) Zoom current (d)Power.

The time range for SP3 spans from 1.6s to 2.0s, indicating a PV insolation of 390 (W/m²) to 40 (W/m2) during observation. In the final configuration, both the PV system and battery system are utilized to effectively manage the load. This comprehensive examination is intended to offer insights into the system's performance under various loads, emphasizing key performance indicators and numerical data for a thorough assessment. The simulation results for voltage, current, and power for the three configurations are elaborately presented in Figure 16, with power details tabulated in Table 6, outlining the discharge battery and DC drive power of the proposed algorithms.

Table 6. Simulation results.

Configuration	Insolation (W/m²)	PV Power (Watts)		Battery Power (Watts)		Load Power (Watts)	
		SMC	SMC-CNN	SMC	SMC-CNN	SMC	SMC-CNN
SP1 (Dis-Charge)	30	10.25	12.25	292.59	293.50	203.89	225.89
	200	121.50	124.68	281.41	292.90	203.87	231.54
	320	270.21	282.26	241.85	292.24	225.169	232.76
	380	316.855	328.68	235.06	293.61	200.44	227.43
SP2 (Charge)	587	441.97	464.04	-272.14	-265.57	196.52	234.46
	677	473.93	504.81	-273.09	-266.57	182.87	234.26
	706	487.15	511.72	-300.93	-305.39	198.95	236.59
	720	502.90	519..45	-300.42	-321.02	203.62	248.57
	680	486.72	503.63	-296.67	-299.67	215.04	241.86
	587	434.83	458.36	289.82	-202.74	206.50	231.90
SP3 (Dis-Charge)	390	332.806	33.70	268.06	286.09	182.69	232.90
	220	151.12	151.12	273.21	273.71	225.74	232.34
	40	12.78	14.62	292.59	292.65	230.77	230.23

 doi:10.20944/preprints202407.0545.v1

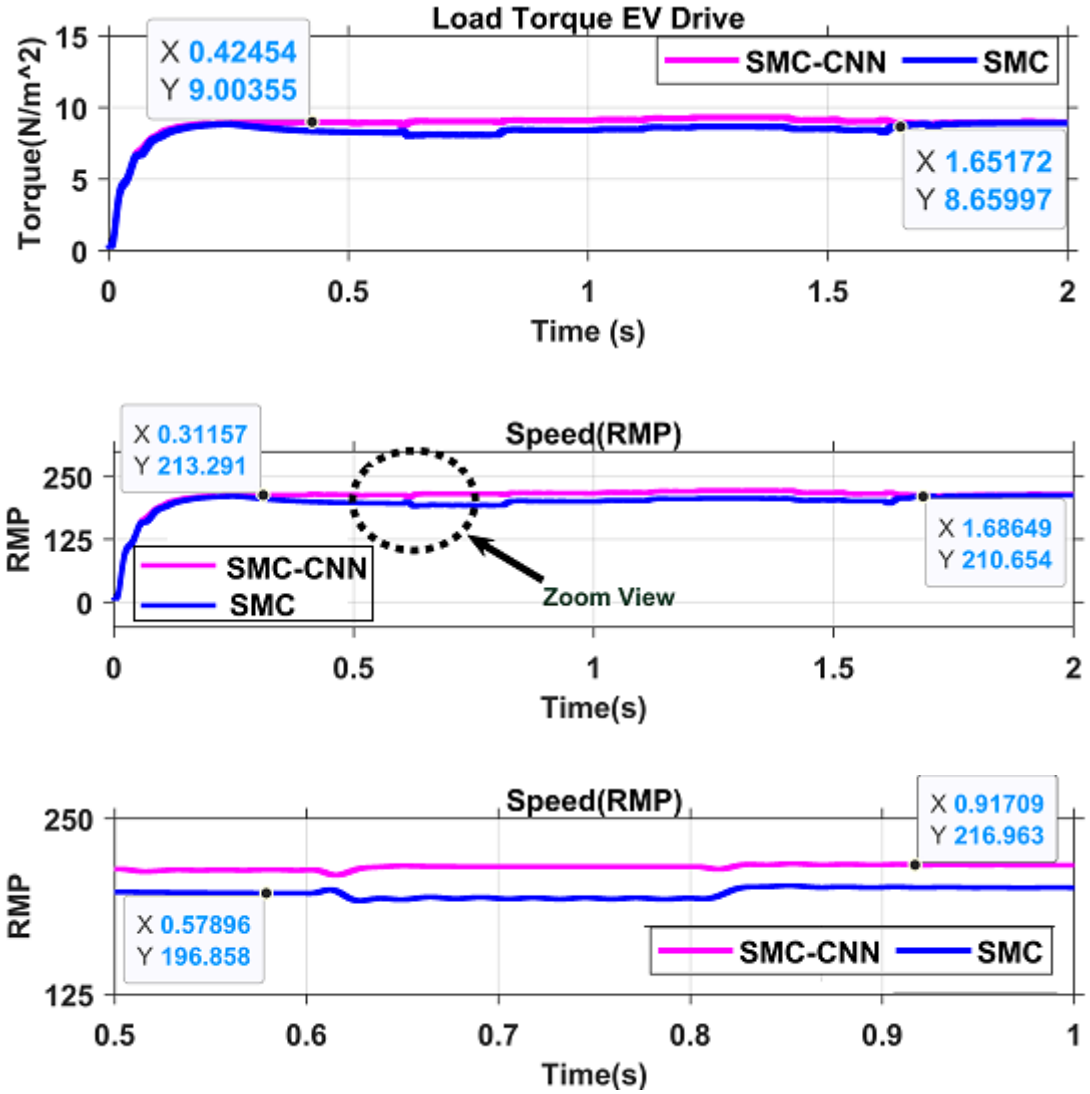

Figure 17. Mechanical Parameter (a) EV Torque (b) EV speed(c)zoom View of speed.

Table 7. Mechanical Parameter.

Configuration	Torque (Nm)		Speed (RPM)	
	SMC	SMC-CNN	SMC	SMC-CNN
SP1	8.354	9.003	204.678	213.291
SP2	8.412	9.096	201.718	216.701
SP3	8.651	8.972	210.654	218.365

The analysis delves further into the drive load voltage, load current, torque, and drive speed values of three major configurations of the SMC and SMC-CNN, as presented in Figures 8 and 9, respectively. Notably, from Table 5, the torque and speed values for the three different configurations of the SMC controller are as follows: torque values of 8.354, 8.412, and 8.65 with corresponding speeds of 204.678, 201.718, and 210.654, respectively. In comparison, the SMC-CNN configurations show torque values of 9.003, 9.096, and 8.972 with corresponding speed responses of 213.291, 216.701, and 218.365, respectively. These results indicate that the SMC-CNN configurations exhibit improved torque and speed values compared to the SMC configurations.

Preprints.org (www.preprints.org) | NOT PEER-REVIEWED | Posted: 5 July 2024 doi:10.20944/preprints202407.0545.v1

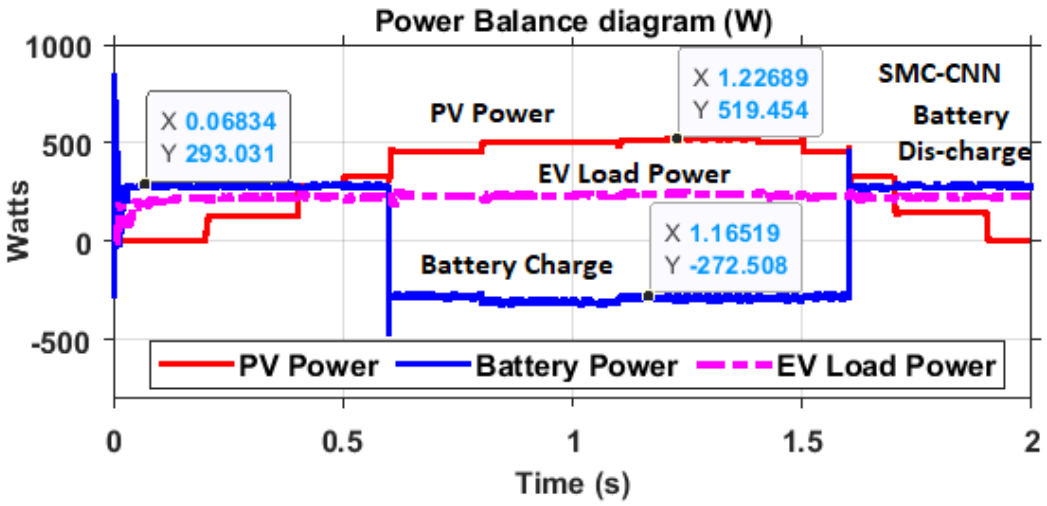

Figure 18. Power Conversion systems.

The Figure 18 shows a power control system for off-grid EV drive applications, connecting the battery and PV arrays to the common DC drive load through separate converters. The photovoltaic (PV) array supplies electricity to both the direct current (DC) load and the battery during the charging process. Once the battery is fully charged, both the battery and PV arrays collectively provide power to the shared DC load. The text outlines battery charging and discharging conditions, power converter control in Mode1, Mode2, and Mode3 operations, and simulation results demonstrating dynamic system response during model changeover.

5. Experimental Verification

The proposed concept underwent assessment and a downsized experimental model was constructed. The created prototype satisfies the specified requirements. It incorporates a battery charging setup comprising two 12V and 35Ah batteries connected in series, with the experimental validation successfully conducted. Figure 19 depicts a graphical portrayal of the proposed system.

The power electronics of a versatile power electronic prototype kit are equipped with open terminals, allowing for the integration of both the boost converter and bidirectional converter. The user has the flexibility to connect the power electronic switches and other components as needed. To ensure isolation between the control circuit and power circuit, the IC MCT2E is utilized for optical isolation.

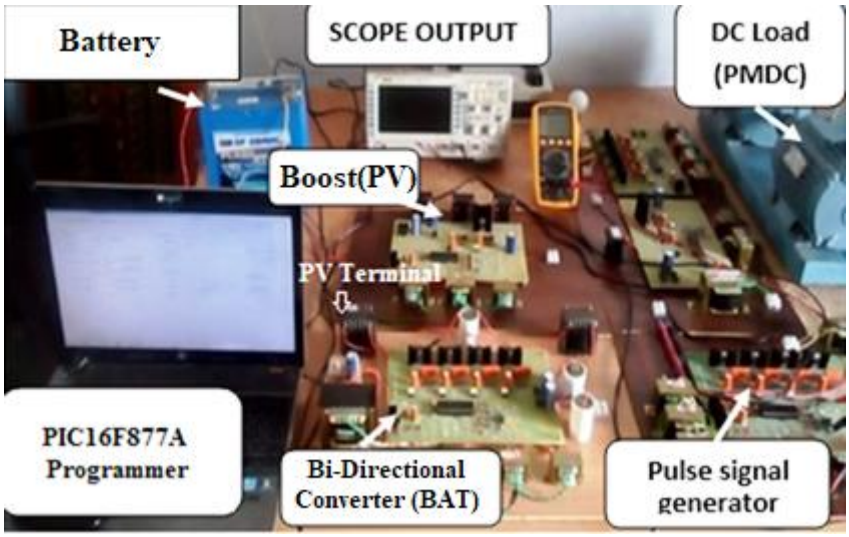

Figure 19. DC link current from the hybrid SPV.

Preprints.org (www.preprints.org) | NOT PEER-REVIEWED | Posted: 5 July 2024 doi:10.20944/preprints202407.0545.v1

The MOSFET is controlled by the switching pulses illustrated in Figure 19. The Opto Isolator IC MCT2E facilitates the transmission of these switching pulses to the MOSFET gate. During the experimental procedure, the solar irradiance was modified from 200 w/m2 to 720 w/m2 using an artificial setup, resulting in the solar PV current depicted in Figure 20. The SMC algorithm, integrated into the PIC 16F877A microcontroller, regulates the switching pulses shown in Figure 21.

Figure 20. DC link current from the SPV.

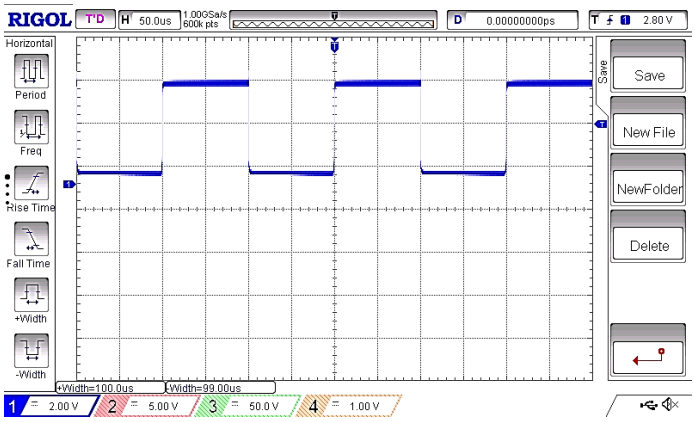

Figure 21. The switching pulses converter.

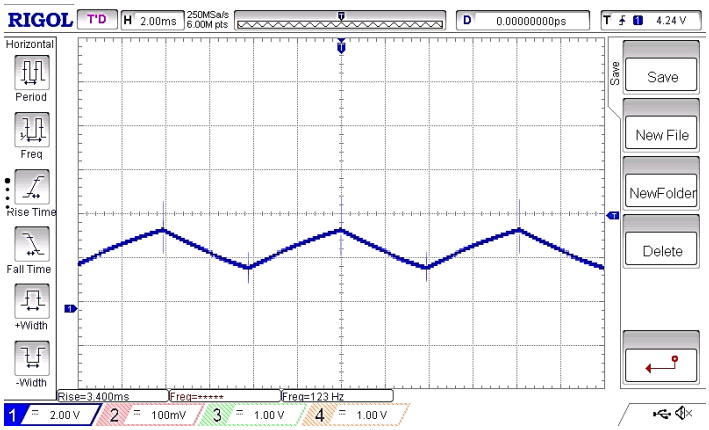

Figure 22. The PV converter inductor current.

Preprints.org (www.preprints.org) | NOT PEER-REVIEWED | Posted: 5 July 2024 doi:10.20944/preprints202407.0545.v1

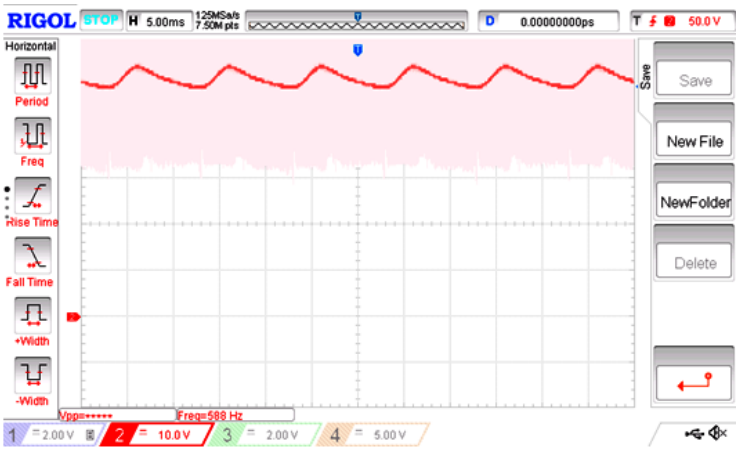

Figure 23. The battery current through the inductor.

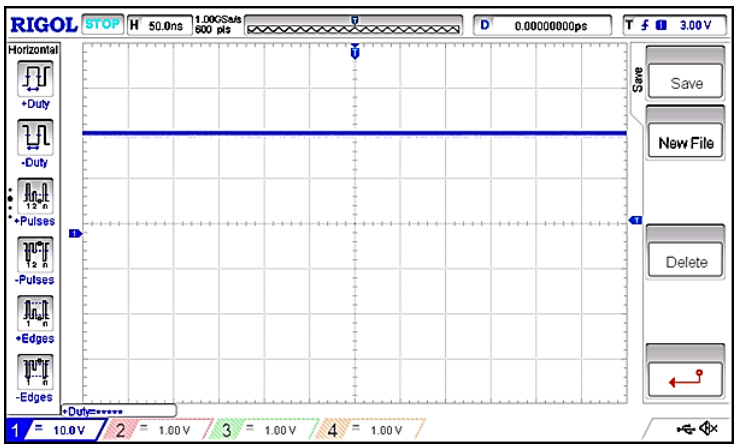

Figure 24. The PV panel terminal Voltage.

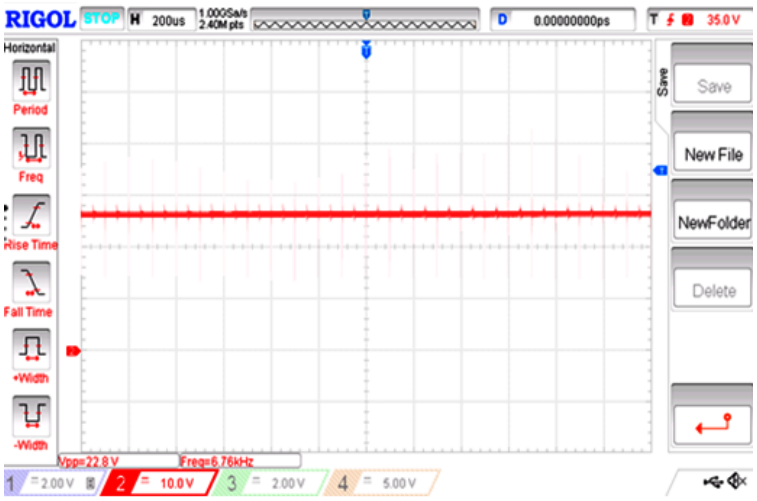

Figure 25. The terminal Voltage of the PV panel.

The abrupt alteration in solar irradiance has been noted to cause a rise in the DC link current, consequently boosting the power supplied to the EV drive for battery integration. The resulting current passing through the inductor (L) of the PV boost converter and the bidirectional battery is

 doi:10.20944/preprints202407.0545.v1

illustrated in Figures 22 and 23, respectively. Figures 24 and 25 depict the PV voltage and battery voltage across the MOSFET of both the boost and bidirectional converters.

The prototype incorporates a PIC16F877A microcontroller, which allows for the attenuation of input and output voltages and currents. To power the microcontroller and the opto couplers, a DC power supply is obtained from separate 230 V/9 V transformers. It is important to note that the DC supplies for the opto couplers are unregulated, while the microcontroller receives a controlled 5 VDC power supply. The control programmer's hex codes are generated in a C language programming environment after establishing the necessary wiring configuration based on the specific application requirements.

6. Conclusions

This article introduces an innovative artificial intelligence technique, known as SMC-CNN, which is applied to the charging process of a lithium-ion battery within an Electric Vehicle Charging optimal operation framework. The effectiveness of charging the battery in various operational modes is confirmed by the simulation results. Specifically, the focus is on the battery's capacity to quickly charge at increased recharge rates. The research draws from a real-life project and includes specific details. For instance, meteorological data is utilized in the design of photovoltaic (PV) panels, and the daily energy requirements of the electric vehicle (EV) are considered to identify the optimal capacity for the battery storage system. A comprehensive analysis of these aspects is essential for a comprehensive comprehension of the system's behavior.

Author Contributions:

Funding:

Conflicts of Interest:

References

1. Haque, M. R., Salam, K. M. A., &Razzak, M. A. (2023).' A modified PI-controller based high current density DC–DC converter for EV charging applications'. IEEE Access, 11, 27246-27266.
2. Ragasudha, C. P., and Hemamalini, S. (2024). 'Performance Analysis of a High Gain Bidirectional DC-DC Converter Fed Drive for an Electric Vehicle with Battery Charging Capability During Braking'. IEEE Access.
3. RajabiA.,Rajaei,A.,Tehrani,.V.m., Dehghhanian,p.,Guerrero,J.M., and Kahan,B.,(2022), 'A non-isolated high step-up DC-DC converter using voltage lift technique: analysis, design, and implementation'., IEEE Access, 10, 6338-6347
4. Benlahbib, B., Bouarroudj, N., Mekhilef, S., Abdeldjalil, D., Abdelkrim, T., &Bouchafaa, F. (2020). Experimental investigation of power management and control of a PV/wind/fuel cell/battery hybrid energy system micro grid. International Journal of Hydrogen Energy, 45(53), 29110-29122.
5. Ahmad, A., Reza, M. M., Beig, A. R., Alsawalhi, J. Y., & Al Jaafari, K. (2022). High voltage gain switched-z-source bidirectional dc-dc converter. IEEE Access, 10, 53560-53577.
6. Velić, T., Becher, Y., &Parspour, N. (2023). 'A Pareto Based Comparison of DC/DC Converters for Variable DC-Link Voltage in Electric Vehicles'. IEEE Open Journal of Power Electronics, 4, 1011-1024.
7. Mudiyanselage, G. A., Keshmiri, N., &Emadi, A. (2023). 'A Review of DC-DC Resonant Converter Topologies and Control Techniques for Electric Vehicle Applications'. IEEE Open Journal of Power Electronics, 4, 945-964.
8. Khasim, S. R., Dhanamjayulu, C., &Muyeen, S. M. (2023). 'A single inductor multi-port power converter for electric vehicle applications'. IEEE ACCESS, 11, 3367-3385.
9. Keshmiri, N., Mudiyanselage, G. A., Chakkalakkal, S., Kozielski, K., Pietrini, G., &Emadi, A. (2022). 'Design and control methodology of a three-port resonant converter for electric vehicles'. IEEE Open Journal of the Industrial Electronics Society, 3, 650-662.
10. Ilahi, T., Izhar, T., Qaisar, S. M., Shami, U. T., Zahid, M., Waqar, A., & Alzahrani, A. (2023). 'Design and performance analysis of ultra-wide band gap power devices-based EV fast charger using bi-directional power converters'. IEEE Access, 11, 25285-25297.

11. Hou, N., Li, Y., Quan, Z., Li, Y. W., & Zhou, A. (2021). 'Unified fast-dynamic direct-current control scheme for intermediary inductive AC-link isolated DC-DC converters'. IEEE Open Journal of Power Electronics, 2, 383-400.
12. B. Dursun and E. Aykut, (2019) , 'An investigation on wind/PV/fuel cell/battery hybrid renewable energy system for nursing home in Istanbul," Proceedings of the Institution of Mechanical Engineers', Journal of Power and Energy, vol. 233, no. 5, pp. 616–625, 2019.
13. W. Jing, C. H. Lai, D. K. Ling, W. S. H. Wong, and M. D. Wong, (2019), 'Battery lifetime enhancement via smart hybrid energy storage plug-in module in standalone photovoltaic power system', Journal of Energy Storage, vol. 21, pp. 586–598.
14. M. Alramlawi, A. Gabash, E. Mohagheghi, and P. Li, 'Optimal operation of hybrid PV-battery system considering grid scheduled blackouts and battery lifetime', *Solar Energy*, vol. 161, pp. 125–137, 2018.
15. Singh, P., & Lather, J. S. (2020). 'Variable structure control for dynamic power-sharing and voltage regulation of DC microgrid with a hybrid energy storage system'.International Transactions on Electrical Energy Systems,30(9), e12510..
16. J. Kathiresan, S. K. Natarajan, and G. Jothimani, (2020), 'Energy management of distributed renewable energy sources for residential DC microgrid applications', Int Trans Electrical energy systemt, vol. 30, no. 3, e12258. .
17. S. Kosai, (2019),'Dynamic vulnerability in standalone hybrid renewable energy system',Energy Conversion and Management, vol. 180, pp. 258–268.
18. L. Luo, S. S. Abdulkareem, A. Rezvani et al.,(2020), 'Optimal scheduling of a renewable based microgrid considering photovoltaic system and battery energy storage under uncertainty," Journal of Energy Storage', Vol. 28, Article ID 101306.
19. M. P. Bonkile and V. Ramadesigan, (2019), 'Power management control strategy using physics-based battery models in standalone PV-battery hybrid systems', Journal of Energy Storage, vol. 23, pp. 258–268.
20. M. Alowaifeer and A. S. Meliopoulos, (2019)'Centralized microgrid energy management system based on successive linearization', NAPS, pp. 1–6.
21. M. G M Abdolrasol, M. A. Hannan, S. M. S. Hussain, T. S. Ustun, M. R. Sarker, and P. J. Ker, 'Energy management scheduling for microgrids in the virtual power plant system using artiJcial neural networks', Energies, vol. 14, no. 20, p. 6507, 2021.
22. A. Salazar, D. Arcos-Aviles, J. Llanos et al., 'Model predictive control-based energy management system for isolated electro thermal micro grids in rural areas of Ecuador', European Conference on Power Electronics and Applications, pp. 1–6, Ghent, Belgium, September 2021.
23. K. A. Al Sumarmad, N. Sulaiman, N. I. A. Wahab, and H. Hizam, 'Energy management and voltage control in microgrids using artiJcial neural networks', PID, and fuzzy logic controllers," Energies, vol. 15, no. 1, p. 303, 2022.
24. X. Zhang, L. Liu, Y. Dai, and T. Lu, "Experimental investigation on the online fuzzy energy management of hybrid fuel cell/battery power system for UAVs," International Journal of Hydrogen Energy, vol. 43, no. 21, pp. 10094–10103, 2018.
25. P. Bhowmik, S. Chandak, and P. K. Rout, 'State of charge and state of power management in a hybrid energy storage system by the self-tuned dynamic exponent and the fuzzy-based dynamic PI controller', International Transactions on Electrical Energy Systems, vol. 29, no. 5, 2019.
26. H. Assem, T. Azib, F. Bouchafaa, A. Hadj Arab, and C. Laarouci,(2020), 'Limits control and energy saturation management for DC bus regulation in photovoltaic systems with battery storage',*Solar Energy*, vol. 211, pp. 1301–1310.